

## Article

# Insight into the Physicochemical Properties of Co-Based Catalysts in Fischer–Tropsch Synthesis

Nothando C. Shiba <sup>1,\*</sup>, Xinying Liu <sup>2</sup> and Yali Yao <sup>2,\*</sup>

<sup>1</sup> Department of Chemical Engineering, Florida Campus, University of South Africa, Roodepoort 1710, South Africa

<sup>2</sup> Institute for Development of Energy for African Sustainability (IDEAS), Florida Campus, University of South Africa, Roodepoort 1710, South Africa; liux@unisa.ac.za

\* Correspondence: eshibanc@unisa.ac.za or shibacynthia@gmail.com (N.C.S.); yaoy@unisa.ac.za (Y.Y.)

**Abstract:** The effect of the different supports and catalyst-reducing agents on the Fischer–Tropsch (FT) reaction was investigated. The large surface area SiO<sub>2</sub> support with a smaller pore volume deposited fine, evenly distributed Co<sub>3</sub>O<sub>4</sub>. Cubic-shaped Co<sub>3</sub>O<sub>4</sub> appeared in clusters on the TiO<sub>2</sub> support, whereas Co<sub>3</sub>O<sub>4</sub> existed as single large particles on the Al<sub>2</sub>O<sub>3</sub> support. The activity data obtained were discussed in terms of cluster size, particle size, particle shape, and mass transport limitations. The SiO<sub>2</sub>-supported catalysts showed a higher activity for the formation of paraffinic products when reduced in H<sub>2</sub> at 250 °C. This is attributed to the formation of the CoO-Co active bond, which enhanced the activation of CO and the hydrogenation reactions. A higher activity was observed for the TiO<sub>2</sub>-supported catalyst at a higher reduction temperature (350 °C) when the mass of Co metal was higher. It afforded more paraffinic products due to enhanced secondary hydrogenation of olefins at higher reaction rates. The large Co<sub>3</sub>O<sub>4</sub> supported on Al<sub>2</sub>O<sub>3</sub> showed the least activity at both reduction temperatures due to strong metal-support interactions. The H<sub>2</sub>-reduced catalysts exhibited superior activity compared to all the syngas-reduced catalysts. Syngas reduction led to surface carbon deposition and the formation of surface carbides which suppressed the hydrogenation reactions and are selective to olefinic products.

**Keywords:** CO hydrogenation; cobalt support; H<sub>2</sub> activation; syngas activation; Fischer–Tropsch synthesis



**Citation:** Shiba, N.C.; Liu, X.; Yao, Y. Insight into the Physicochemical Properties of Co-Based Catalysts in Fischer–Tropsch Synthesis. *Reactions* **2023**, *4*, 420–431. <https://doi.org/10.3390/reactions4030025>

Academic Editor: Wenping Ma

Received: 11 May 2023

Revised: 11 July 2023

Accepted: 31 July 2023

Published: 4 August 2023



**Copyright:** © 2023 by the authors. Licensee MDPI, Basel, Switzerland. This article is an open access article distributed under the terms and conditions of the Creative Commons Attribution (CC BY) license (<https://creativecommons.org/licenses/by/4.0/>).

## 1. Introduction

For many decades, Fischer–Tropsch synthesis (FTS) has been the leading technology used in the production of alternative clean fuels from syngas derived from coal, biomass, and natural gas. Even though this process has been extensively studied for over 100 years and is now well-established, the selectivity for targeted products remains a challenge [1,2]. Amongst other techniques, catalyst synthesis and pre-treatment have been employed to optimize the selectivity of the FTS process. The preferred catalysts for the FTS process are cobalt (Co) and iron (Fe) supported catalysts, due to their high activity, good stability, and low selectivity to CO<sub>2</sub> [3]. Despite the considerable amount of literature on catalyst synthesis and pre-treatment, their effect on cobalt dispersion, dynamic atomic structure, and catalyst activity is still not yet understood. Understanding the precursor transformation into active catalysts under different atmospheres is very crucial for FTS selectivity and activity when using heterogenous catalysts [4,5].

Interactions between the Co precursor and the oxide support such as Al<sub>2</sub>O<sub>3</sub>, SiO<sub>2</sub>, and TiO<sub>2</sub> have been reported to dramatically affect the H<sub>2</sub>/CO adsorption, reduction, carburization, and FTS performance of cobalt catalysts [6]. These interactions change the electronic and geometric structure of the active component thus inducing different activities due to a different charge transfer, nanoparticle morphology, chemical composition, surface

acidity, etc. [7,8]. TiO<sub>2</sub> has been reported to exhibit a particular type of metal–support interactions, in this case, strong metal–support interactions (SMSI) with group IIIV metals. The strong metal–support interactions originate from the reduction of titania, which leads to the formation of intermetallic compounds and electron transfer and the formation of an oxide layer over the active phase, which has a detrimental effect on the overall performance of the catalyst [7–10]. Hong et al. [6] coated the TiO<sub>2</sub> support with carbon nitride (CN) to weaken metal–support interactions and reported that CN hindered the diffusion of reduced titania species over cobalt nanoparticles, which in turn enhanced the dispersion and stabilization of Co nanoparticles. Rapid deactivation was observed on the uncoated Co/TiO<sub>2</sub> catalyst, which was attributed to the formation of TiO<sub>2</sub> coating over the cobalt species [6]. Kliewer et al. [11] suggested that during the reduction of cobalt, the TiO<sub>2</sub> support is partially reduced to TiO<sub>2-x</sub>, and this migrates onto the support metal particles and blocks the active sites. The authors reported a loss of activity for the Co-Re/TiO<sub>2</sub> catalyst stemming from the strong metal interactions and accumulative cobalt surface TiO<sub>2</sub> decoration [11].

Similar to TiO<sub>2</sub>, the Al<sub>2</sub>O<sub>3</sub> support is known to exhibit strong metal–support interactions with the active phase, which forms aluminates, which are usually difficult to reduce and inert for the FTS reaction [12–14]. Tasavoli et al. [15] studied the regeneration of deactivated Co-Ru/Al<sub>2</sub>O<sub>3</sub> catalysts and found that water-induced oxidation of cobalt can be completely reversed at temperatures of 270–275 °C in an H<sub>2</sub> flow and the generated cobalt–alumina interactions can also be regenerated at temperatures closer to the first reduction step. However, the formation of cobalt aluminates can only be reversed at temperatures above 800 °C. In total, 29% total catalyst activity was recovered at 400 °C for the Co-Ru/Al<sub>2</sub>O<sub>3</sub> catalyst and about 7.2% total irreversible loss of activity due to aluminates formation together with sintering and coke deposition. In accordance, Tsakoumis et al. [16] suggested that the diffusion of Co atoms into the support takes place during calcination, which leads to the formation of irreducible compounds and the reoxidation of smaller (<5.3 nm) Co nanoparticles followed by Co oxide spreading. This results in the formation of Co<sub>x</sub>Al<sub>y</sub>O<sub>z</sub> phases during the initial stage of the reaction and in irreversible loss of activity. Spreading CoO<sub>x</sub> species over the SiO<sub>2</sub> support during FTS has been discussed previously [17,18]. The relatively weak interaction between Co and SiO<sub>2</sub> had a positive effect on the formation of Co-CoO active composite, which promoted the FT reaction and the secondary hydrogenation of olefins to paraffins [18]. SiO<sub>2</sub> usually exhibits weak metal–support interactions compared to TiO<sub>2</sub> and Al<sub>2</sub>O<sub>3</sub>, which leads to a high Co reducibility and activity [19,20].

Hydrocarbons are formed through a stepwise addition of methyl monomer (CH<sub>x</sub>), produced from CO adsorption, dissociation, and hydrogenation with H<sub>2</sub> on the catalyst metal surface [1]. Pre-treatment in H<sub>2</sub> is therefore essential, in order to convert the supported metal-oxides into metal catalysts. In addition to the standard H<sub>2</sub> activation, CO and syngas have also been used for Co pre-treatment [5,21]. Our previous study [21] demonstrated that reducing a cobalt catalyst in a syngas environment favored the production of olefins due to the formation of Co<sub>x</sub>C species, which suppressed the hydrogenation reactions. 1-Olefins are formed from the primary reactions and can re-absorb on the catalyst surface to form metal alkyl and undergo competitive reactions, i.e., (i) hydrogenation to produce paraffin (ii) dehydrogenation to 1-olefins (iii) hydrogenolysis and (iv) reinsertion to produce larger hydrocarbons [22–24]. Secondary re-adsorption and reinsertion of 1-olefins result in higher hydrocarbons; therefore, controlling the pathway of secondary reactions becomes important for increasing the selectivity of higher hydrocarbons [22].

Pan et al. [25] studied the activation of Co/ZnO in CO, syngas, and CO followed by syngas (CO/SG). A low CO conversion and a high methane selectivity were observed over the CO-activated catalyst, due to the formation of bulk cobalt carbide and cobalt oxide which favored the hydrogenation of 1-olefins and increased methane production. Similar trends were observed in previous studies where methane was primarily produced on the cobalt carbide surface via CO activation [26,27]. The CO/SG-activated catalyst showed the

highest activity and selectivity due to the formation of Co(hcp), which has a high intrinsic activity relative to Co(fcc) obtained via H<sub>2</sub> activation [25].

In summary, although the catalytic performance of cobalt supported on the traditional supports (SiO<sub>2</sub>, TiO<sub>2</sub>, and Al<sub>2</sub>O<sub>3</sub>) has been thoroughly investigated, the effect of activation conditions on different supports remains controversial. In our opinion, some of the variations reported in the literature may be due to different conditions used during catalyst preparation, reduction, and FTS. Consequently, the purpose of the present study was to investigate the role of support in a highly systematic way, so the reaction and reduction conditions were kept the same while the support, reducing agent, and reducing temperature were varied. This eliminates any additional factors that may affect the activity of the catalysts and ensure a thorough understanding of the reaction behavior brought about by changing one factor at a time. Here, we report the selectivity obtained over SiO<sub>2</sub>, TiO<sub>2</sub>, and Al<sub>2</sub>O<sub>3</sub>-supported cobalt catalysts, which were pre-treated in both H<sub>2</sub> and syngas prior to the FTS reaction at temperatures between 250–350 °C.

## 2. Experimental

Catalysts containing 15 wt% cobalt on metal oxide (TiO<sub>2</sub>, SiO<sub>2</sub>, and Al<sub>2</sub>O<sub>3</sub>) were prepared by adding deionized water to metal-oxide to form a mixture, followed by the addition of cobalt nitrate hexahydrate (Co(NO<sub>3</sub>)<sub>2</sub>·6H<sub>2</sub>O, Sigma-Aldrich, Johannesburg, South Africa, 99.0%) mixture, followed by drying at 40–110 °C and calcination at 350 °C for 8 h. Details of the preparation have been provided elsewhere [21]. The morphology of the prepared catalysts was observed using a transmission electron microscope (TEM). TEM measurements were taken using a JEOL 2010F instrument operating at 200 KV. The average particle size and particle size distribution were determined by TEM images by counting more than 100 particles. Brunauer–Emmett–Teller (BET) surface area and porosity data were collected using a Micrometrics Trista 3000 analyzer. 0.2 g of each sample was degassed prior to analysis at 190 °C for 8 h. The pore size distribution for each sample was evaluated based on the desorption branches on the isotherms using the Barrett–Joyner–Halenda (BJH) method, while the total pore volume was determined at a relative pressure of 0.99. The BET was used to study the loss/gain of the surface area for all catalyst samples after calcination, as shown in Table 1. X-ray diffraction (XRD) of the fresh samples was performed using a Siemens D5000 X-ray diffractometer with Cu K $\alpha$  radiation (40 kV, 30 mA). The measurements were recorded from 10 to 90 degrees in the 2 $\theta$  range using a step size of 0.020° and a step time of 12 s for all samples. The crystallite size of Co<sub>3</sub>O<sub>4</sub> was calculated using the Scherrer equation and assuming spherical particles.

**Table 1.** The physical properties, activation conditions, and reaction conditions of the supported catalysts.

Catalyst	Co/SiO <sub>2</sub>	Co/TiO <sub>2</sub>	Co/Al <sub>2</sub> O <sub>3</sub>
<b>Catalyst Characterization Data</b>			
BET surface area for the support [m <sup>2</sup> /g]	456.5	24.15	107.5
BET surface area after calcination [m <sup>2</sup> /g]	407.0	88.4	115.8
TEM Co <sub>3</sub> O <sub>4</sub> particle size [nm]	26	28	38
XRD Co <sub>3</sub> O <sub>4</sub> particle size [nm] <sup>b</sup>	17	22	33
XRD Co <sup>0</sup> crystallite size [nm] <sup>c</sup>	12.8	16.5	24.8
BET pore size [nm]	6.78	38.1	43.1
<b>Catalyst reduction conditions</b>			
Temperature (°C)	250 or 350		
Reduction agents	H <sub>2</sub> or syngas (H <sub>2</sub> /CO/N <sub>2</sub> = 60/30/10)		
<b>FTS reaction conditions</b>			
Feed gas	syngas (H <sub>2</sub> /CO/N <sub>2</sub> = 60/30/10)		
Temperature (°C)	220		
Pressure (bar)	20		
Flowrate (Nml/min)	60		

<sup>b</sup> XRD Co<sub>3</sub>O<sub>4</sub> particle size calculated from the Scherrer equation [6]. <sup>c</sup> Co<sup>0</sup> crystallite size calculated from the Scherrer equation  $d_{Co^0} = 0.75 \times d_{Co_3O_4}$  [2].

Catalyst activity evaluation was carried out in three fixed-bed reactors (ID = 8 mm). The catalyst was first sieved into particles less than 200  $\mu\text{m}$  and one gram of the sieved catalyst was loaded in each reactor and pre-treated in either  $\text{H}_2$  or syngas (30%  $\text{CO}$ , 60%  $\text{H}_2$ , balance  $\text{N}_2$ ) at a temperature range of 250–350  $^\circ\text{C}$  prior to the FTS reaction. The FTS reaction was carried out at 220  $^\circ\text{C}$ , 20 bar, and 60  $\text{Nml}/\text{min}$  in syngas feed composition of 30%  $\text{CO}$ , 60%  $\text{H}_2$ , and 10%  $\text{N}_2$ . Periodic samples of the gas phase were analyzed using an Agilent gas chromatograph (GC) 7890A equipped with two thermal conductivity detectors (TCDs) to analyze the inorganic gases and one flame ionization detector (FID) to analyze the hydrocarbon products, operating at 220  $^\circ\text{C}$ . The feed gas is converted to hydrocarbons during FTS and product yield and selectivity are given on a carbon basis. We calculated the  $\text{CO}$  conversion and the rate of formation of a gas product ( $\theta_i$ ) using Equations (1) and (2) following the terms % $\text{CO}$  and % $X$ , respectively.

$$\% \text{CO} = \frac{F_{in} X_{co, in} - F_{out} X_{co, out}}{F_{in} X_{co, in}} \quad (1)$$

where  $X_{co, in}$  is the molar fraction of % $\text{CO}$  in the reactor inlet gas feed;  $X_{co, out}$  is the molar fraction of % $\text{CO}$  in the reactor outlet gas stream;  $F_{in}$  is the total molar flow rate of the reactor inlet gas feed, mol/min; and  $F_{out}$  is the total molar flow rate of the reactor outlet gas stream, mol/min.

$$\% r_{\theta_i} = \frac{F_{out} X_{\theta_i, out}}{m_{cat}} \quad (2)$$

where  $X_{\theta_i, out}$  is the molar fraction of  $\theta_i$  in the reactor outlet gas stream.

### 3. Results

The effect of three supports ( $\text{SiO}_2$ ,  $\text{TiO}_2$ , and  $\text{Al}_2\text{O}_3$ ) on the catalytic activity of Co-based catalysts was evaluated. Figure 1 shows the TEM images of the fresh catalysts. The  $\text{TiO}_2$ -supported catalyst showed a relatively spatial distribution of  $\text{Co}_3\text{O}_4$  particles on the cubic-shaped support, see Figure 1a. The  $\text{SiO}_2$  catalyst showed fine, evenly distributed spherical  $\text{Co}_3\text{O}_4$  particles (Figure 1b). With the  $\text{Al}_2\text{O}_3$  support,  $\text{Co}_3\text{O}_4$  is mostly seen to be as larger single particles, see Figure 1c. The Co particle sizes ranged from 26–38 nm, in the order of  $\text{Co}/\text{SiO}_2 < \text{Co}/\text{TiO}_2 < \text{Co}/\text{Al}_2\text{O}_3$ , see Table 1. Larger Co particles (>12 nm) have been reported to exhibit a high degree of reduction and to favor the readsorption of  $\alpha$ -olefins and the production of heavy hydrocarbon [4].

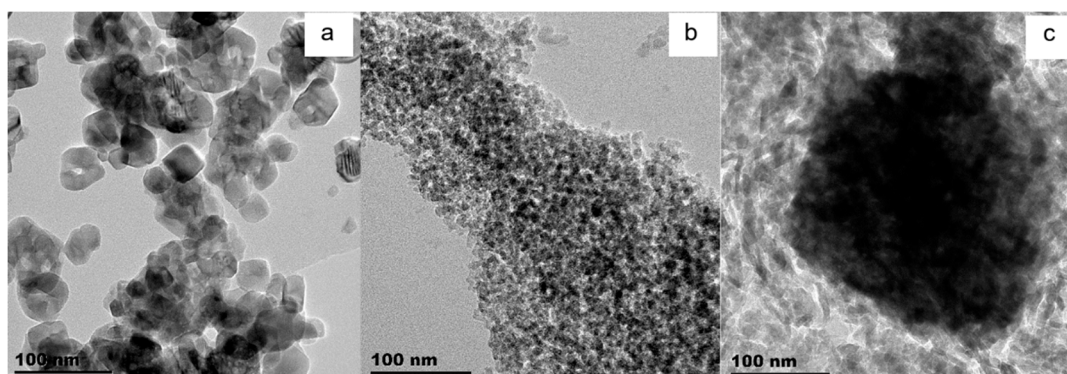


**Figure 1.** TEM results for the fresh supported catalysts taken at 100 nm for all samples (a)  $\text{TiO}_2$ ; (b)  $\text{SiO}_2$ ; and (c)  $\text{Al}_2\text{O}_3$ .

The XRD patterns for the various supported cobalt catalysts after calcination are shown in Figure 2. The  $\text{Co}/\text{TiO}_2$  catalyst has a cubic spinel structure (Figure 1a), thus showing very strong, intense diffractions of cobalt oxide compared to  $\text{Al}_2\text{O}_3$  and  $\text{SiO}_2$ , respectively, (Figure 2). Both the  $\text{Al}_2\text{O}_3$  and  $\text{TiO}_2$ -supported catalysts show interaction with cobalt oxide at diffraction peaks 45 $^\circ$  and 65 $^\circ$  for  $\text{Al}_2\text{O}_3$  and at a range of 65–70 $^\circ$

for  $\text{TiO}_2$ , suggesting the formation of irreducible compounds and strong metal-support interactions during calcination. The  $\text{SiO}_2$  catalyst diffraction patterns show a lack of cobalt oxide peaks, which is attributed to the amorphous silica phase obtained at low calcination temperatures  $<550^\circ\text{C}$ , which may be due to the weak metal-support interactions inhibiting the crystallization of cobalt nanoparticles. Previous reports investigating the metal-support interactions indicate that  $\text{SiO}_2$  has the least metal-support interactions followed by  $\text{TiO}_2$  and lastly  $\text{Al}_2\text{O}_3$  [6–10]. This is in agreement with our findings over the cobalt catalysts, the stronger the interactions the higher the formation of irreducible compounds, observed via XRD, Figure 2. The  $\text{Co}/\text{SiO}_2$  diffractogram showed a broad shoulder around  $23^\circ$  which can be assigned to the amorphous silica and a peak around  $37\text{--}38^\circ$  which can be attributed to the  $\text{Co}_3\text{O}_4$  phase. Previous studies observed the broad peak at  $23^\circ$  when using  $\text{SiO}_2$  as a support [28]. Notably, the peaks at  $32^\circ$ ,  $38^\circ$ ,  $45^\circ$ ,  $58^\circ$ , and  $75^\circ$  on the  $\text{TiO}_2$  catalyst and  $38^\circ$ ,  $45^\circ$ , and  $58^\circ$  on the  $\text{Al}_2\text{O}_3$  catalyst are attributed to  $\text{Co}_3\text{O}_4$  crystals.

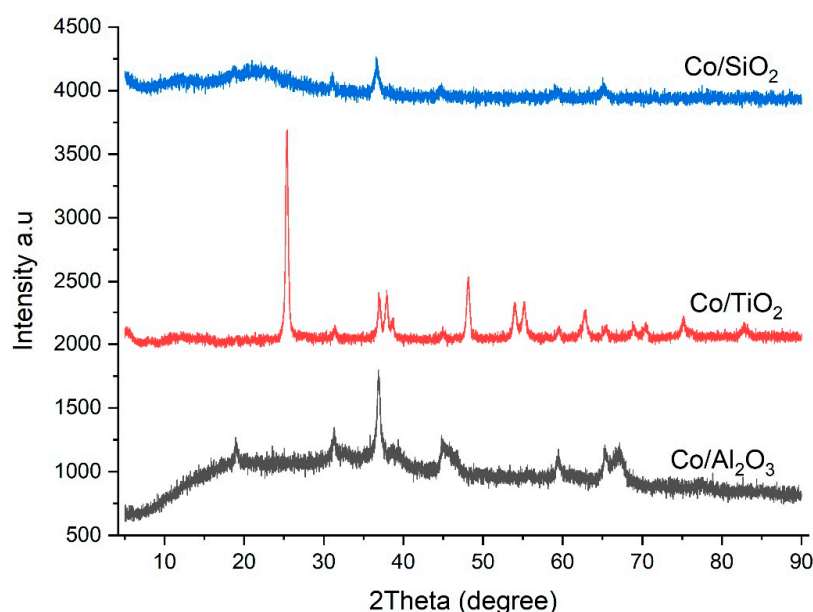


**Figure 2.** XRD results for the fresh supported catalysts after calcination:  $\text{Co}/\text{SiO}_2$ ;  $\text{Co}/\text{TiO}_2$ ; and  $\text{Co}/\text{Al}_2\text{O}_3$ .

The Scherrer equation was used to calculate the average  $\text{Co}_3\text{O}_4$  crystallite size (see, Table 1) [6] and to obtain the corresponding cobalt metal ( $\text{Co}^0$ ) crystallite size, the calculated thickness value is multiplied by 0.75, which is based on the molar ratio of cobalt and oxygen in  $\text{Co}_3\text{O}_4$  [2]. The results in Table 1 indicate that there is a direct correlation between the XRD  $\text{Co}_3\text{O}_4$  crystallite size and the BET average pore diameter of the support rather than the type of support used. The  $\text{Co}_3\text{O}_4$  crystallite size was found to be smaller for a small BET average pore size support, which is in line with our finding over the TEM results in Table 1 and with previous studies [2,3].

The BET surface area of the support materials and the catalysts after impregnation are summarized in Table 1. The BET surface area for the oxide catalysts is in the range of  $88\text{--}407\text{ m}^2/\text{g}$ . It was found that the loss of surface area after calcination depended on the size of the  $\text{Co}_3\text{O}_4$  particle: The smaller the particle size, the more surface area that is lost, as is evident in the  $\text{Co}/\text{SiO}_2$  samples. The loss of surface area can be attributed to the pores being filled with impregnated cobalt species. This is due to silica migration, which occurs at temperatures higher than  $300^\circ\text{C}$  and with a surface area higher than  $>200\text{ m}^2/\text{g}$  [29]. The large  $\text{SiO}_2$  surface area inhibited the agglomeration of the  $\text{Co}_3\text{O}_4$  particles, resulting in an even distribution, as shown in Figure 1b. The  $\text{SiO}_2$  catalyst showed the largest surface area with a smaller pore volume, thus leading to a smaller  $\text{Co}_3\text{O}_4$  average particle size.

This is in line with previously reported studies on the  $\text{SiO}_2$  catalyst [28,29]: The particle size was found to increase with a decrease in surface area and an increase in the pore volume.

For the  $\text{Co}/\text{TiO}_2$  and  $\text{Co}/\text{Al}_2\text{O}_3$  catalysts, an increase in the BET surface area was observed after calcination. This may be due to larger  $\text{Co}_3\text{O}_4$  particles settling on the surface of the catalyst. The  $\text{TiO}_2$  and  $\text{Al}_2\text{O}_3$  catalysts precursors also exhibited a higher porosity compared to  $\text{SiO}_2$ , which may mean that the pores are more closely connected. This may enhance the possibility of diffusion into adjacent pore cavities and decrease the distance between the cobalt particles, which may, in turn, further increase the probability of cluster growth, which is more visible on the  $\text{TiO}_2$  catalysts (Figure 1a) due to the shorter diffusion distance.

The BET isotherms for nitrogen adsorption and desorption obtained with the cobalt-based catalysts are shown in Figure 3. The  $\text{SiO}_2$ -supported catalyst with the highest BET surface area ( $407.0 \text{ m}^2/\text{g}$ ), Figure 3, can be classified as type IV, according to the IUPAC classification. Type IV corresponds to mesoporous materials, which is corroborated by the presence of the hysteresis loop (H1 type according to IUPAC classification). The H1 type represents porous materials that consist of well-defined cylindrical pore channels or agglomerates of uniform spheres [30]. This is in line with the spherical cobalt nanoparticles deposited on the  $\text{SiO}_2$  support observed via TEM (Figure 1b) and with the amorphous silica structure observed via XRD (Figure 2). Another study observed the type IV isotherm for  $\text{SiO}_2$  and modified  $\text{SiO}_2$  with chelating agents [28], which was attributed to the mesoporous  $\text{SiO}_2$  material. The  $\text{TiO}_2$ - and  $\text{Al}_2\text{O}_3$ -supported catalysts, Figure 3, respectively, correspond to the type III IUPAC classification for macroporous materials [30]. The  $\text{TiO}_2$  and  $\text{Al}_2\text{O}_3$  type III IUPAC classification reflects on the broader pore size distribution, see Table 1.

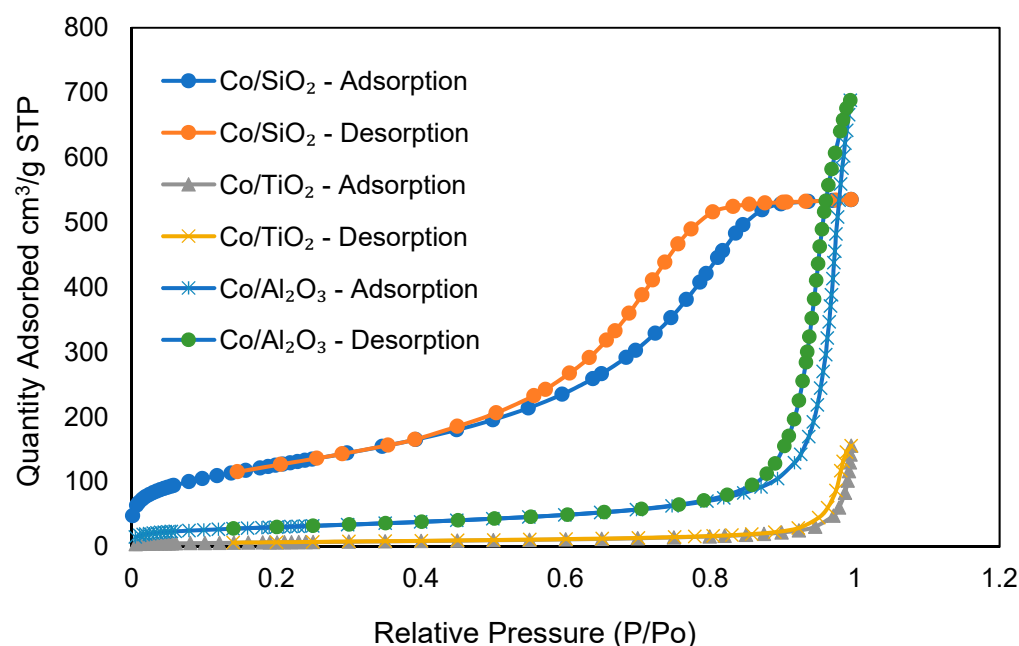


**Figure 3.** BET adsorption and desorption isotherms for the cobalt catalysts after calcination;  $\text{Co}/\text{SiO}_2$  catalyst;  $\text{Co}/\text{TiO}_2$  catalyst; and  $\text{Co}/\text{Al}_2\text{O}_3$  catalyst.

The FTS reaction was conducted in a fixed-bed microreactor at  $220 \text{ }^\circ\text{C}$  and 20 bars for all catalyst samples. The performance parameters recorded after reaching a steady state are provided in Figures 4–6. The  $\text{SiO}_2$ -supported catalyst reduced in  $\text{H}_2$  exhibited the highest CO reaction rate at a lower reduction temperature ( $250 \text{ }^\circ\text{C}$ ) (Figure 4a), while the  $\text{TiO}_2$ -supported catalysts reduced in  $\text{H}_2$  showed higher activity at  $350 \text{ }^\circ\text{C}$  with respect to  $\text{SiO}_2$ - and  $\text{Al}_2\text{O}_3$ -supported catalysts. (See Figure 4b).

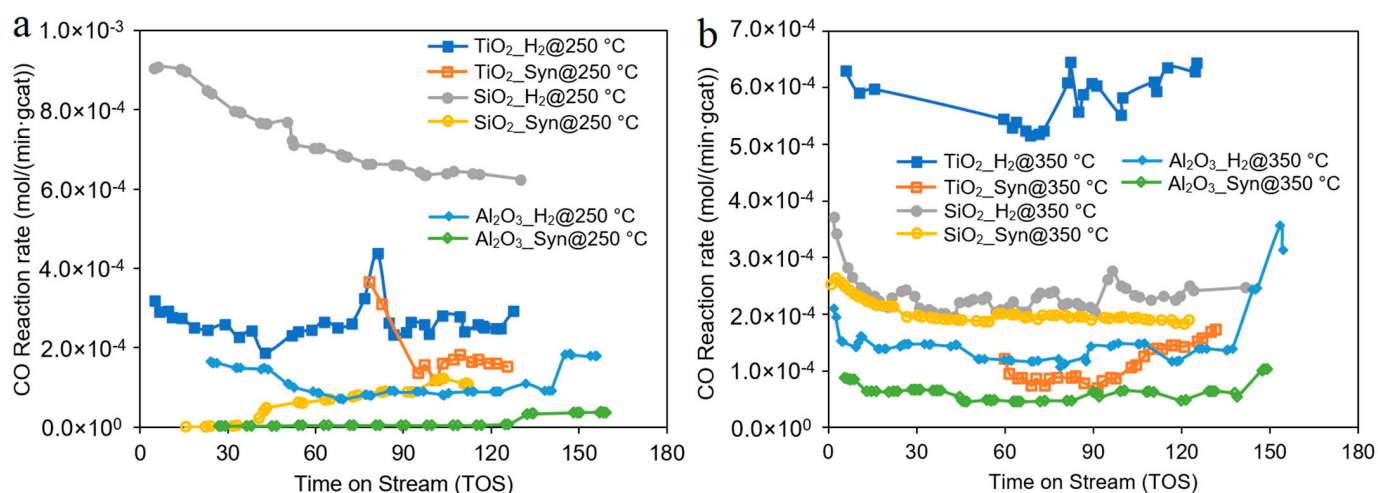


**Figure 4.** CO reaction rates (mol/min/g catalyst) at a gas hourly space velocity (GHSV) of 3600 Nml/h/gCat with time on stream for: (a) Catalysts reduced in H<sub>2</sub> or syngas at 250 °C (H<sub>2</sub>@250 or Syn@250 °C) and (b) catalysts reduced in H<sub>2</sub> or syngas at 350 °C (H<sub>2</sub>@350 or Syn@350 °C).

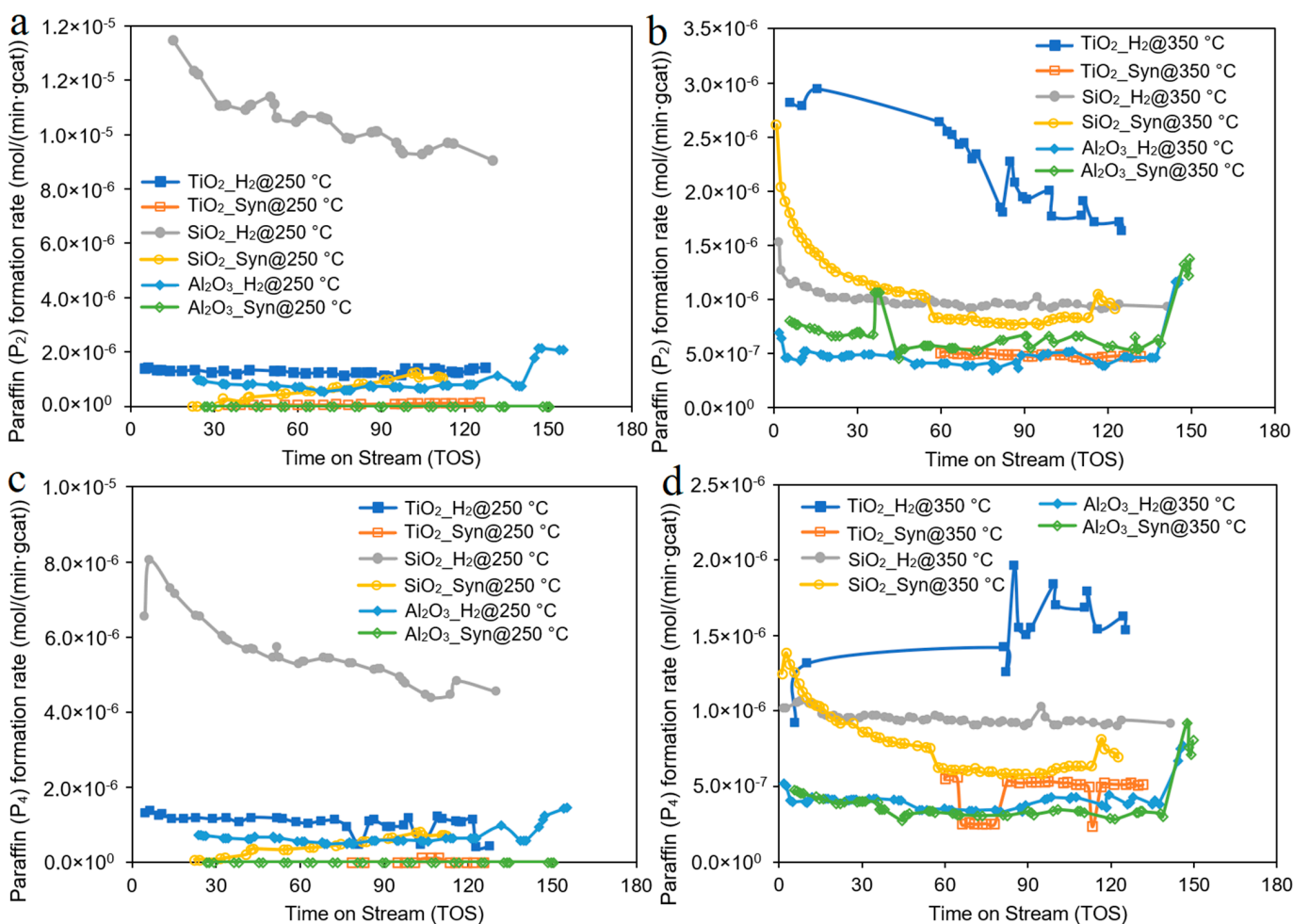


**Figure 5.** Paraffin formation rates (mol/min/g catalyst) with TOS when the catalyst was reduced in H<sub>2</sub> or syngas at different reduction temperatures and at a GHSV of 3600 Nml/h/gCat: (a) ethane (P<sub>2</sub>) reduced at 250 °C; (b) P<sub>2</sub> reduced at 350 °C; (c) butane (P<sub>4</sub>) reduced at 250 °C; (d) P<sub>4</sub> reduced at 350 °C.

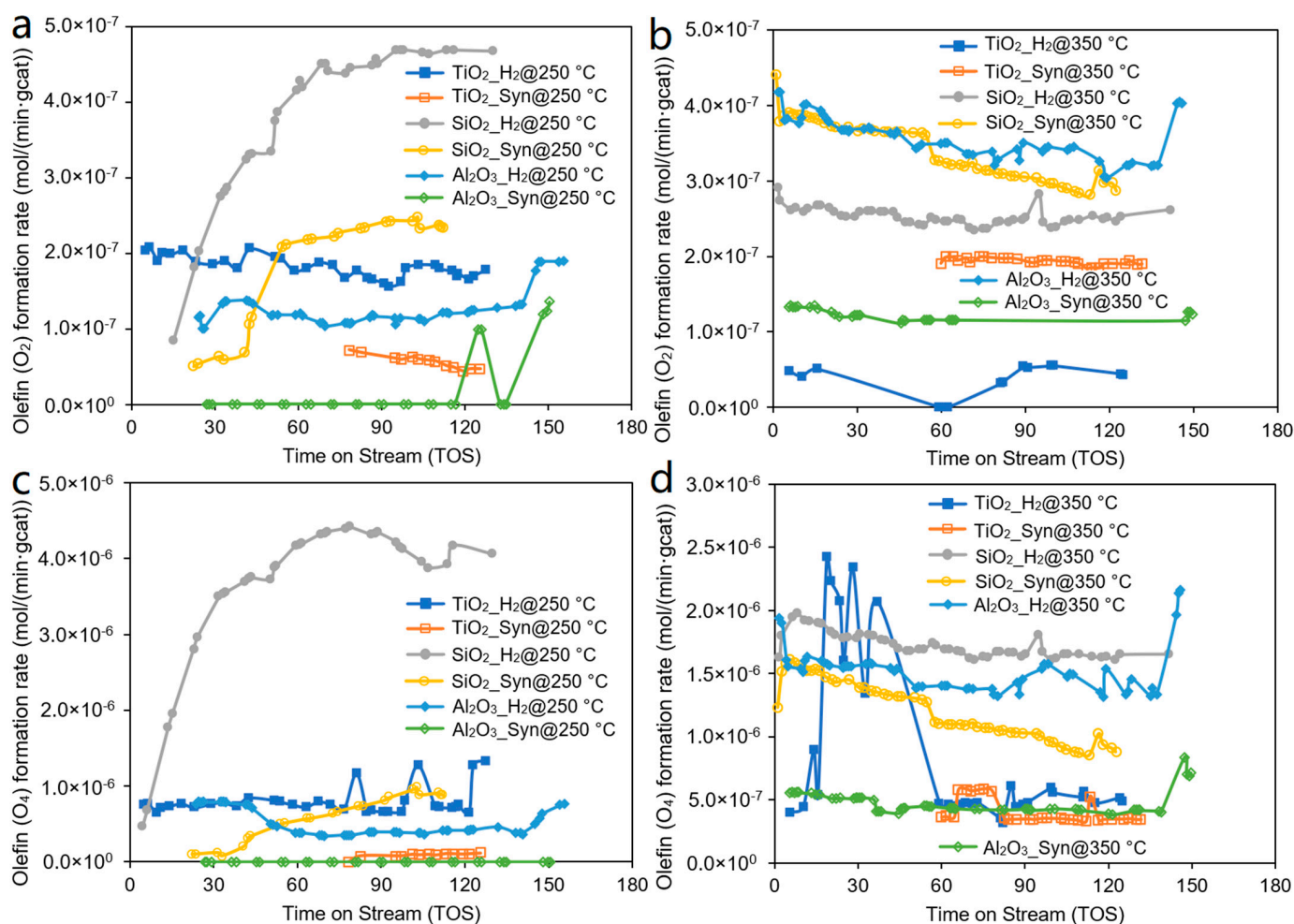


**Figure 6.** Olefin formation rates with TOS at different reduction temperatures and at a GHSV of 3600 Nml/h/gCat: (a) Ethene (O<sub>2</sub>) when the catalysts reduced in H<sub>2</sub> or syngas at 250 °C; (b) O<sub>2</sub> when the catalysts reduced in H<sub>2</sub> or syngas at 350 °C; (c) butene (O<sub>4</sub>) when the catalysts reduced in H<sub>2</sub> or syngas at 250 °C; and (d) O<sub>4</sub> when the catalysts reduced in H<sub>2</sub> or syngas at 350 °C.

Our previous study [18] proved that the small-particle Co<sub>3</sub>O<sub>4</sub> catalysts formed an active CoO-Co-SiO<sub>2</sub> interface when they reduced the catalyst in H<sub>2</sub> at 250 °C, resulting in enhanced activity and selectivity of paraffinic products (see Figure 5a,c). An increase in the hydrogenation of 1-olefins led to the formation of paraffinic products at higher CO reaction rates. Furthermore, the research [18] indicated that the synergy between the CoO- and Co-assisted the activation of CO to monomers for enhanced FT activity or reacted with the hydrocarbon precursor to form paraffins. The opposite trend in activity and selectivity was observed at 350 °C. This suggests that an increase in the reduction temperature might have led to the agglomeration of the small cobalt catalysts and increased the metal-support interaction between the Co<sub>3</sub>O<sub>4</sub> and SiO<sub>2</sub>, resulting in fewer active phases than when it is partially reduced.

The TiO<sub>2</sub>-supported catalyst was not as active as the SiO<sub>2</sub> catalyst at 250 °C, but it showed the best performance when the catalyst reduced in H<sub>2</sub> at 350 °C (Figure 4b). This may be attributed to the encapsulation of metallic Co by TiO<sub>2-x</sub> as a result of the lower surface free energy of the latter and may suggest the wetting of TiO<sub>2</sub> by CoO [6]. It is well known that spherical Co metal is the active phase for FTS [31]. Therefore, the cubic shape might have lowered the amount of Co-CoO<sub>x</sub> phase formed on the low surface area TiO<sub>2</sub>. The FTS reaction is shape-sensitive and -selective, so the spreading of the CoO<sub>x</sub> on the surface of the cubic TiO<sub>2</sub> particles might have been deposited on one side only. Figure 5 shows the formation rate of ethane (P<sub>2</sub>) and butane (P<sub>4</sub>) paraffinic products against time

on stream. The TiO<sub>2</sub> catalysts showed higher paraffin selectivity at 350 °C than SiO<sub>2</sub> and Al<sub>2</sub>O<sub>3</sub>. This can be attributed to transport restrictions imposed by the physical structure of the support and by a high Co site density within the catalyst pellets, which increases the residence time and the re-adsorption probability of reactive  $\alpha$ -olefins, thus leading to a higher yield of paraffinic products. The TiO<sub>2</sub> catalyst was more selective to olefins when reduced at a lower temperature, see Figure 6a,c. A low reduction temperature leads to incomplete reduction of the Co<sub>3</sub>O<sub>4</sub>. Our previous research [21] indicates that reducing at 250 °C in H<sub>2</sub> results in a mixture of Co<sub>3</sub>O<sub>4</sub>, CoO, and Co and that reducing in syngas, produces a mixture of Co<sub>3</sub>O<sub>4</sub>, Co<sub>x</sub>C, CoO, C, and sometimes Co<sup>0</sup>. Furthermore, cobalt oxides are reported to favor the production of short-chain hydrocarbons [4]; therefore, the TiO<sub>2</sub> catalyst was more selective to olefins due to incomplete reduction and a high mass percentage of cobalt oxides.

The Al<sub>2</sub>O<sub>3</sub>-supported catalyst showed the least activity and was more selective to olefinic products at both reduction temperatures used—see Figure 6. This may be due to the strong metal-support interactions associated with the Al<sub>2</sub>O<sub>3</sub> support, which is detrimental to the activity of the catalyst. In addition, the strong metal-support interactions inhibited the complete reduction of Co<sub>3</sub>O<sub>4</sub> to Co metal, which resulted in the production of olefins and shorter-chain hydrocarbons. Cobalt oxides have previously been reported to inhibit chain growth and to be inactive for FTS [4]. Furthermore, the Al<sub>2</sub>O<sub>3</sub> catalyst deposited very large Co<sub>3</sub>O<sub>4</sub> particles (38 nm), and the FTS reaction is known to be a very sensitive reaction with a preferable Co particle size of about 10 nm for higher activity. Very large Co<sub>3</sub>O<sub>4</sub> particles have been reported to affect the selectivity of Co catalysts negatively, which results in more olefinic products and shorter chain hydrocarbons [4,32]. Our findings for the Al<sub>2</sub>O<sub>3</sub> catalyst are in line with this.

All H<sub>2</sub>-reduced samples surpassed the activity of the syngas-reduced catalysts, which suggests that the Co metal is the most active phase for Co-FTS. The syngas-reduced catalysts showed higher selectivity towards olefins due to the formation of cobalt carbides, an active phase for olefin production, and the deposition of surface carbon. The Co<sub>x</sub>C phase has also been widely reported to hinder the hydrogenation reaction [4,21], and hence the observed low activity for all syngas-reduced catalysts compared to H<sub>2</sub> reduction.

Table 2 shows the activity and selectivity of the supported cobalt catalysts under study with respect to previously reported catalysts. Saib et al. [33] achieved a higher CO conversion, about 44%, for a Co/SiO<sub>2</sub> catalyst reduced at 350 °C in H<sub>2</sub> with a higher methane and lower C<sub>5+</sub> selectivity, compared to the model catalyst under study (which achieved about 26%). (See Table 2). This can be attributed to the higher Co loading and higher reaction temperature used in the Saib et al. study. Diehl et al. [34] and Jalama et al. [35] achieved lower activity for the supported cobalt catalysts on TiO<sub>2</sub>, reduced at 350 and 250 °C, respectively, compared to the model TiO<sub>2</sub> catalysts under study. Furthermore, Park et al. [36] reported very low activity of about 4% (Table 2) for an Al<sub>2</sub>O<sub>3</sub>-supported catalyst reduced at 350 °C. This may be attributed to the different levels of Co loading, and the different reducing and reaction conditions, which may alter the physiochemical properties of the catalysts and so lead to different catalytic performance results, rendering the selectivity comparison prone to errors. This elucidates the requirement for a systematic way of keeping the reduction and reaction conditions the same in order to make comparisons without introducing too many variations. There is also little information available on the effect of support materials on the activity and selectivity of cobalt-based catalysts reduced at lower temperatures, i.e., 250 °C.

**Table 2.** Activity and selectivity results for the 15% Co model catalysts, with activation conditions of 250/350 °C, 1 bar, and H<sub>2</sub>, and reaction conditions of H<sub>2</sub>/CO = 2, 210 °C, 20 bar, and GHSV of 3600 Nml/h/gCat.

Catalyst	Reducing T	CO%	CH <sub>4</sub> %	CH <sub>2-4</sub> %	C <sub>5+</sub> %	Comments
Co/SiO <sub>2</sub>	250 °C	69	23	14.9	62	This work.
	350 °C	26	9	8.8	82	This work.
	350 °C	44	12	—	71	Data from Ref [33], reaction conditions: 220 °C, 15 bar, and GHSV = 1 (NTP)/h.g with 20% Co loading.
	250 °C	31	12	6.9	81	This work.
	350 °C	72	8	3.3	89	This work.
Co/TiO <sub>2</sub>	350 °C	42.6	8.9	—	84.8	Data from Ref [34], reaction conditions: 210 °C, 15 bar and GHSV = 3595 mL/g/h with 10% Co loading with 0.5% Re promotion.
	250 °C	15	3.9	—	92.2	Data from Ref [35], reaction conditions: 220 °C, 15 bar and GHSV = 3 NL/gCat/h with 10% Co loading.
Co/Al <sub>2</sub> O <sub>3</sub>	250 °C	23	25	12.5	62	This work.
	350 °C	42	14	11.2	77	This work.
	350 °C	4.7	14.5	16.8	68.5	Data from Ref [36], reaction T was 240 °C, 9.8 bar and GHSV = 3600 L/kgCat/h with 5% Co loading.

#### 4. Conclusions

A series of promoted cobalt catalysts supported on Al<sub>2</sub>O<sub>3</sub>, SiO<sub>2</sub>, and TiO<sub>2</sub> was studied using different characterization techniques and the FTS reaction. The pore volume and structures were found to influence the size, shape, and appearance of the cobalt particles significantly. On the larger-pore  $\gamma$ -Al<sub>2</sub>O<sub>3</sub> and TiO<sub>2</sub> supports, Co<sub>3</sub>O<sub>4</sub> was found as single particles that were quite evenly distributed, whereas on the smaller SiO<sub>2</sub> pores, spherical Co<sub>3</sub>O<sub>4</sub> exists as finely distributed particles. Despite the smaller pore volume, no agglomeration was observed on SiO<sub>2</sub>, due to the large surface area. The SiO<sub>2</sub> catalysts exhibited the highest activity at 250 °C due to the formation of a unique CoO-Co interface that assisted with the activation of CO and enhanced the secondary hydrogenation reactions for paraffinic products. The TiO<sub>2</sub> catalysts showed cubic-shaped particles that were more active at 350 °C, and its high porosity and low surface area led to the formation of agglomerates with a rather broad cluster size distribution, which might have hindered the FT reaction at 250 °C. The Al<sub>2</sub>O<sub>3</sub> catalyst showed the least activity due to larger metal-support interactions. Syngas reduction favored olefinic products due to the formation of cobalt carbides which are highly selective to olefins, which inhibit the hydrogenation reactions. The structure of the support has a profound effect on the size, shape, and appearance of the Co<sub>3</sub>O<sub>4</sub> particles and the internal structure of these supports is still not completely understood. This work provides a great avenue for future catalyst and FTS reaction design. Overall, better catalyst activity and selectivity were attained with the H<sub>2</sub>-reduced catalysts which reflect the superiority of H<sub>2</sub> as a reducing agent compared to syngas. Furthermore, high surface area supports allow for the use of low reduction temperature, which will potentially cut down energy costs for the FTS system due to the formation of unique Co-CoO active interactions beneficial for the FTS reaction and for the production of paraffins.

**Author Contributions:** Conceptualization, X.L. and Y.Y.; methodology, Y.Y.; software, X.L. and X.L.; validation, N.C.S. and Y.Y.; formal analysis, Y.Y. and N.C.S.; investigation, N.C.S.; resources, X.L.; data curation, N.C.S.; writing—original draft preparation, N.C.S.; writing—review and editing, N.C.S. and Y.Y.; visualization, Y.Y.; supervision, X.L. and Y.Y.; project administration, Y.Y.; funding acquisition, X.L. All authors have read and agreed to the published version of the manuscript.

**Funding:** This research received no external funding.

**Data Availability Statement:** The data presented in this study will be shared upon reasonable request to the corresponding author.

**Conflicts of Interest:** The authors declare that they have no known competing financial interests or personal relationships that could have appeared to influence the work reported in this paper.

## References

1. Sage, V.; Sun, Y.; Hazewinkel, P.; Bhatelia, T.; Braconnier, L.; Tang, L.; Chiang, K.; Batten, M.; Burke, N. Modified product selectivity in Fischer–Tropsch synthesis by catalyst pre-treatment. *Fuel Process. Technol.* **2017**, *167*, 183–192. [[CrossRef](#)]
2. Vosoughi, V.; Badoga, S.; Dalai, A.K.; Abatzoglou, N. Effect of pretreatment on physicochemical properties and performance of multiwalled carbon nanotube supported cobalt catalyst for Fischer–Tropsch Synthesis. *Ind. Eng. Chem. Res.* **2016**, *55*, 6049–6059. [[CrossRef](#)]
3. Mitchell, R.W.; Lloyd, D.C.; van de Water, L.G.A.; Ellis, P.R.E.; Metcalfe, K.A.; Sibbald, C.; Davies, L.H.; Enache, D.I.; Kelly, G.J.; Boyes, E.D.; et al. Effect of pretreatment method on the nanostructure and performance of supported Co catalysts in Fischer–Tropsch synthesis. *ACS Catal.* **2018**, *8*, 8816–8829. [[CrossRef](#)]
4. Shiba, N.C.; Yao, Y.; Liu, X.; Hildebrandt, D. Recent developments in catalyst pretreatment technologies for cobalt based Fischer–Tropsch synthesis. *Rev. Chem. Eng.* **2022**, *38*, 503–538. [[CrossRef](#)]
5. Chang, Q.; Li, K.; Zhang, C.; Cheruvathur, A.V.; Zheng, L.; Yang, Y.; Li, Y. XAFS Studies of Fe–SiO<sub>2</sub> Fischer–Tropsch Catalyst during activation in CO, H<sub>2</sub>, and Synthesis Gas. *ChemCatChem* **2019**, *11*, 2206–2216. [[CrossRef](#)]
6. Hong, J.; Wang, B.; Xiao, G.; Wang, N.; Zhang, Y.; Khodakov, A.Y.; Li, J. Tuning the metal–support interaction and enhancing the stability of titania-supported cobalt Fischer–Tropsch catalysts via carbon nitride coating. *ACS Catal.* **2020**, *10*, 5554–5566. [[CrossRef](#)]
7. Wan, H.; Wu, B.; Xiang, H.; Li, Y. Fischer–Tropsch synthesis: Influence of support incorporation manner on metal dispersion, metal–support interaction, and activities of iron catalysts. *ACS Catal.* **2012**, *2*, 1877–1883. [[CrossRef](#)]
8. Cheng, Q.; Liu, Y.; Lyu, S.; Tian, Y.; Ma, Q.; Li, X. Manipulating metal–support interactions of metal catalysts for Fischer–Tropsch synthesis. *Chin. J. Chem. Eng.* **2021**, *35*, 220–230. [[CrossRef](#)]
9. Bowker, M.; Stone, P.; Morrall, P.; Smith, R.; Bennett, R.; Perkins, N.; Kvon, R.; Pang, C.; Fourre, E.; Hall, M. Model catalyst studies of the strong metal–support interaction: Surface structure identified by STM on Pd nanoparticles on TiO<sub>2</sub> (110). *J. Catal.* **2005**, *234*, 172–181. [[CrossRef](#)]
10. Zhang, Y.; Su, X.; Li, L.; Qi, H.; Yang, C.; Liu, W.; Pan, X.; Liu, X.; Yang, X.; Huang, Y.; et al. Ru/TiO<sub>2</sub> catalysts with size-dependent metal/support interaction for tunable reactivity in Fischer–Tropsch synthesis. *ACS Catal.* **2020**, *10*, 12967–12975. [[CrossRef](#)]
11. Kliewer, C.E.; Soled, S.L.; Kiss, G. Morphological transformations during Fischer–Tropsch synthesis on a titania-supported cobalt catalyst. *Catal. Today* **2019**, *323*, 233–256. [[CrossRef](#)]
12. Pardo-Tarifa, F.; Cabrera, S.; Sanchez-Dominguez, M.; Boutonnet, M. Ce-promoted Co/Al<sub>2</sub>O<sub>3</sub> catalysts for Fischer–Tropsch synthesis. *Int. J. Hydrogen Energy* **2017**, *42*, 9754–9765. [[CrossRef](#)]
13. Liu, Y.; Jia, L.; Hou, B.; Sun, D.; Li, D. Cobalt aluminate-modified alumina as a carrier for cobalt in Fischer–Tropsch synthesis. *Appl. Catal. A Gen.* **2017**, *530*, 30–36. [[CrossRef](#)]
14. Wolf, M.; Fischer, N.; Claeys, M. Formation of metal–support compounds in cobalt-based Fischer–Tropsch synthesis: A review. *Chem. Catal.* **2021**, *1*, 1014–1041. [[CrossRef](#)]
15. Tavasoli, A.; Abbaslou, R.M.M.; Dalai, A.K. Deactivation behavior of ruthenium promoted Co/ $\gamma$ -Al<sub>2</sub>O<sub>3</sub> catalysts in Fischer–Tropsch synthesis. *Appl. Catal. A Gen.* **2008**, *346*, 58–64. [[CrossRef](#)]
16. Tsakoumis, N.E.; Walmsley, J.C.; Rønning, M.; van Beek, W.; Rytter, E.; Holmen, A. Evaluation of reoxidation thresholds for  $\gamma$ -Al<sub>2</sub>O<sub>3</sub>-supported cobalt catalysts under Fischer–Tropsch synthesis conditions. *J. Am. Chem. Soc.* **2017**, *139*, 3706–3715. [[CrossRef](#)]
17. Melaet, G.; Ralston, W.T.; Li, C.S.; Alayoglu, S.; An, K.; Musselwhite, N.; Kalkan, B.; Somorjai, G.A. Evidence of highly active cobalt oxide catalyst for the Fischer–Tropsch synthesis and CO<sub>2</sub> hydrogenation. *J. Am. Chem. Soc.* **2014**, *136*, 2260–2263. [[CrossRef](#)]
18. Shiba, N.C.; Yao, Y.; Forbes, R.P.; Okoye-Chine, C.G.; Liu, X.; Hildebrandt, D. Role of CoO-Co nanoparticles supported on SiO<sub>2</sub> in Fischer–Tropsch synthesis: Evidence for enhanced CO dissociation and olefin hydrogenation. *Fuel Process. Technol.* **2021**, *216*, 106781. [[CrossRef](#)]
19. Li, L.; Yu, F.; Li, X.; Lin, T.; An, Y.; Zhong, L.; Sun, Y. Fischer–Tropsch to olefins over Co<sub>2</sub>C-based catalysts: Effect of thermal pretreatment of SiO<sub>2</sub> support. *Appl. Catal. A Gen.* **2021**, *623*, 118283. [[CrossRef](#)]

20. Jacobs, G.; Das, T.K.; Zhang, Y.; Li, J.; Racoillet, G.; Davis, B.H. Fischer–Tropsch synthesis: Support, loading, and promoter effects on the reducibility of cobalt catalysts. *Appl. Catal. A Gen.* **2002**, *233*, 263–281. [[CrossRef](#)]
21. Shiba, N.C.; Liu, X.; Hildebrandt, D.; Yao, Y. Effect of pre-treatment conditions on the activity and selectivity of cobalt-based catalysts for CO hydrogenation. *Reactions* **2021**, *2*, 258–274. [[CrossRef](#)]
22. Liu, X.; Hamasaki, A.; Honma, T.; Tokunaga, M. Anti-ASF distribution in Fischer–Tropsch synthesis over unsupported cobalt catalysts in a batch slurry phase reactor. *Catal. Today* **2011**, *175*, 494–503. [[CrossRef](#)]
23. Shiba, N.C.; Liu, X.; Yao, Y. Advances in lower olefin production over cobalt-based catalysts via the Fischer–Tropsch process. *Fuel Process. Technol.* **2022**, *238*, 107489. [[CrossRef](#)]
24. Ojeda, M.; Nabar, R.; Nilekar, A.U.; Ishikawa, A.; Mavrikakis, M.; Iglesia, E. CO activation pathways and the mechanism of Fischer–Tropsch synthesis. *J. Catal.* **2010**, *272*, 287–297. [[CrossRef](#)]
25. Pan, Z.; Parvari, M.; Bukur, D.B. Fischer–Tropsch synthesis on Co/ZnO—Two step activation procedure for improved performance. *Appl. Catal. A Gen.* **2014**, *480*, 79–85. [[CrossRef](#)]
26. Li, J.; Xu, L.; Keogh, R.; Davis, B. Fischer–Tropsch synthesis: Effect of CO pretreatment on a ruthenium promoted Co/TiO<sub>2</sub>. *Catal. Lett.* **2000**, *70*, 127–130. [[CrossRef](#)]
27. Yang, J.; Jacobs, G.; Jermwongratanachai, T.; Pendyala, V.R.; Ma, W.; Chen, D.; Holmen, A.; Davis, B.H. Fischer–Tropsch synthesis: Impact of H<sub>2</sub> or CO activation on methane selectivity. *Catal. Lett.* **2014**, *144*, 123–132. [[CrossRef](#)]
28. Hasanudin, H.; Asri, W.R.; Fanani, Z.; Adisti, S.J.; Hadiyah, F.; Maryana, R.; Al Muttaqii, M.; Zhu, Z.; Machado, N.T. Facile fabrication of SiO<sub>2</sub>/Zr Assisted with EDTA complexed-impregnation and templated methods for crude palm oil to biofuels conversion via catalytic hydrocracking. *Catalysts* **2022**, *12*, 1522. [[CrossRef](#)]
29. Kababji, A.H.; Joseph, B.; Wolan, J.T. Silica-supported cobalt catalysts for Fischer–Tropsch synthesis: Effects of calcination temperature and support surface area on cobalt silicate formation. *Catal. Lett.* **2009**, *130*, 72–78. [[CrossRef](#)]
30. Alothman, Z.A. A review: Fundamental aspects of silicate mesoporous materials. *Material* **2012**, *5*, 2874–2902. [[CrossRef](#)]
31. Claeys, M. Cobalt gets in shape. *Nature* **2016**, *538*, 44–45. [[CrossRef](#)]
32. Rytter, E.; Holmen, A. On the support in cobalt Fischer–Tropsch synthesis—Emphasis on alumina and aluminates. *Catal. Today* **2016**, *275*, 11–19. [[CrossRef](#)]
33. Saib, A.M.; Claeys, M.; Van Steen, E. Silica supported cobalt Fischer–Tropsch catalysts: Effect of pore diameter of support. *Catal. Today* **2002**, *71*, 395–402. [[CrossRef](#)]
34. Diehl, F.; Khodakov, A.Y. Promotion of cobalt Fischer–Tropsch catalysts with noble metals: A review. *Oil Gas Sci. Technol.* **2009**, *64*, 11–24. [[CrossRef](#)]
35. Jalama, K.; Kabuba, J.; Xiong, H.; Jewell, L.L. Co/TiO<sub>2</sub> Fischer–Tropsch catalyst activation by synthesis gas. *Catal. Commun.* **2012**, *17*, 154–159. [[CrossRef](#)]
36. Park, J.Y.; Lee, Y.J.; Karandikar, P.R.; Jun, K.W.; Ha, K.S.; Park, H.G. Fischer–Tropsch catalysts deposited with size-controlled Co<sub>3</sub>O<sub>4</sub> nanocrystals: Effect of Co particle size on catalytic activity and stability. *Appl. Catal. A Gen.* **2012**, *411*, 15–23. [[CrossRef](#)]

**Disclaimer/Publisher’s Note:** The statements, opinions and data contained in all publications are solely those of the individual author(s) and contributor(s) and not of MDPI and/or the editor(s). MDPI and/or the editor(s) disclaim responsibility for any injury to people or property resulting from any ideas, methods, instructions or products referred to in the content.